IOPscience iopscience.iop.org

Home Search Collections Journals About Contact us My IOPscience

The behaviour of resonances in Hecke triangular billiards under deformation

This article has been downloaded from IOPscience. Please scroll down to see the full text article.

2007 J. Phys. A: Math. Theor. 40 9275

(http://iopscience.iop.org/1751-8121/40/31/007)

View the table of contents for this issue, or go to the journal homepage for more

Download details:
IP Address: 171.66.16.144
The article was downloaded on 03/06/2010 at 06:07

Please note that terms and conditions apply.

IOP Publishing Journal of Physics A: Mathematical and Theoretical

J. Phys. A: Math. Theor. **40** (2007) 9275–9295 doi:10.1088/1751-8113/40/31/007

The behaviour of resonances in Hecke triangular billiards under deformation

P J Howard[1] **and P F O'Mahony**

Department of Mathematics, Royal Holloway, University of London, Egham, Surrey TW20 0EX, UK

E-mail: p.howard@qmul.ac.uk and p.omahony@rhul.ac.uk

Received 9 May 2007, in final form 25 June 2007
Published 19 July 2007
Online at stacks.iop.org/JPhysA/40/9275

Abstract

The right-hand boundary of Artin's billiard on the Poincaré half-plane is continuously deformed to generate a class of chaotic billiards which includes fundamental domains of the Hecke groups $\Gamma(2, n)$ at certain values of the deformation parameter. The quantum scattering problem in these open chaotic billiards is described and the distributions of both real and imaginary parts of the resonant eigenvalues are investigated. The transitions to arithmetic chaos in the cases $n \in \{4, 6\}$ are closely examined and the explicit analytic form for the scattering matrix is given together with the Fourier coefficients for the scattered wavefunction. The $n = 4$ and 6 cases have an additional set of regular equally spaced resonances compared to Artin's billiard ($n = 3$). For a general deformation, a numerical procedure is presented which generates the resonance eigenvalues and the evolution of the eigenvalues is followed as the boundary is varied continuously which leads to dramatic changes in their distribution. For deformations away from the non-generic arithmetic cases, including that of the tiling Hecke triangular billiard $n = 5$, the distributions of the positions and widths of the resonances are consistent with the predictions of a random matrix theory.

PACS numbers: 05.45.Pq, 03.65.Nk

1. Introduction

The motion of a particle on a surface of constant negative curvature serves as a paradigm for classical chaotic motion. The motion exhibits the highest degree of chaos possible being both Bernouillian and hyperbolic. In fact, Artin's investigations [1] of a billiard on such a surface

[1] Present address: School of Mathematical Sciences, Queen Mary, University of London, Mile End Road, London E1 4NS, UK.

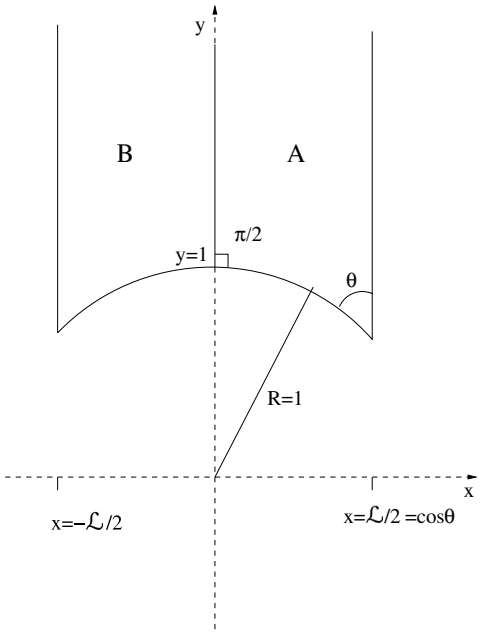

Figure 1. Region A is the triangular billiard system on the Poincaré half-plane that is considered here. The angles of the triangle are $\theta, \pi/2$ and 0. The full region $A + B$ is a fundamental domain for a Hecke group, at values of $\theta = \frac{\pi}{n}, n > 2 \in \mathbb{Z}$.

established the use of symbolic dynamics in classifying dynamical systems. There is a much richer structure to the hyperbolic plane compared to the Euclidean plane where there exist only a finite number of discrete groups together with their fundamental domains which tile the whole plane. For the hyperbolic plane, there exist an infinite number of discrete groups. For each of the fundamental domains of these groups, we can define a billiard system. The most famous of these is Artin's billiard whose fundamental domain is shown in figure 1 for $\theta = \pi/3$.

Being so widely and precisely studied in terms of classical mechanics meant that billiard systems in hyperbolic geometry were natural candidates for an investigation of quantum chaos. For billiard systems which are a fundamental domain of some group, there is in fact an explicit trace formula, Selberg's trace formula, which allows, in principle, the exact calculation of quantum energy eigenvalues from classical quantities such as periodic orbits derived from the group matrices [2]. This exact formula is the analogue of the asymptotic Gutzwiller trace formula for quantum systems in the semi-classical limit of $\hbar \to 0$.

For bound quantum systems defined by these hyperbolic billiards, it was expected that energy level spacing statistics would follow the predictions of random matrix theory (RMT) for a completely chaotic system. Surprisingly, the computed level spacing statistics for Artin's billiard and some other fundamental domains obeyed a Poissonian distribution typical of fully integrable systems [3]. However, other billiard systems showed the expected fit to the distribution for the Gaussian orthogonal ensemble (GOE) of random matrices [4]. It was not until several years later that an explanation for these deviations was forthcoming. In fact, the unexpected statistics only occur in billiard systems which are the *fundamental domain* of some *arithmetic group* [5, 6] which led to the term 'arithmetic chaos' [5] being introduced to

categorize these systems. Bogomolny *et al* [4] showed that the Poissonian statistics could be understood in terms of the exponentially large number of degenerate periodic orbits, i.e. all with the same period, which arise in such systems.

Much as bounded hyperbolic billiard systems should serve as a prototype for bounded quantum systems, open hyperbolic domains should serve the same purpose for quantum chaotic scattering. However, whereas a lot of work has been done on calculating the bound states for hyperbolic systems, much less is known about the complex eigenvalues for the resonances in the continuum. In this paper, we perform an analysis of the resonance spectrum for a whole class of hyperbolic triangular billiards which includes several arithmetic Hecke billiards. Starting from Artin's billiards which is an arithmetical case and where the scattering matrix is known analytically [7], we continuously deform the billiard by moving one of the vertical walls, i.e. by changing $\mathcal{L}$ and hence θ in figure 1, and we trace out how the distribution of resonances change by calculating the resonance positions. As the position of the wall varies, we encounter two other arithmetical Hecke triangular billiards, i.e. for $\theta = \pi/n$ where $n = 4$ or 6 (Artin's billiard corresponds to $n = 3$ in figure 1), and we give the derivation of the scattering matrix in these cases where an additional set of equally spaced resonances are found compared to Artin's billiard. The generic behaviour predicted by RMT for chaotic scattering with a single open channel, the case considered in this paper, is that the level spacing statistics for the real parts of the resonance positions should be distributed as in the GOE and the imaginary parts or the widths of the resonances should follow the Porter–Thomas or chi-squared distribution [8]. We find that this appears generally to be so for deformations away from the three arithmetical cases mentioned above.

The scattering theory for arithmetic systems violates the expectations for generic chaotic systems even more dramatically than the statistics of the bound states do. In particular, for Artin's billiard the resonance positions are determined by the zeros of Riemann's zeta function on the *critical line* $\mathrm{Re}(z) = \frac{1}{2}$ [7]. This leads to two distinct features of the resonance spectrum. First, assuming the Riemann hypothesis, then the imaginary parts of the momenta are all equal to $-\frac{1}{4}$. Second, the statistics of the real parts of the resonant momenta are given by the values of the Riemann zeros and follow the statistics of a Gaussian unitary ensemble (GUE) which is typical of chaotic systems that are not invariant under the operation of time-reversal, although this symmetry is intact in the system. In addition, for arithmetic billiards, there is an infinite set of bound states superimposed on the scattering continuum (so-called 'cusp forms' in mathematics). Such states arise in atomic scattering when the parameters of a system conspire to give zero coupling to the continuum, and are extremely sensitive to perturbation of those parameters [9]. Here, the cusp forms are treated as a part of the resonance continuum as a conjecture by Phillips and Sarnak [10] states that only arithmetic groups should possess such an infinite set of cusp forms and that for arbitrary deformations of the underlying group, they should immediately acquire negative imaginary parts in their energy and thus show up as resonances. So to follow the resonance distributions consistently under deformation we must include the cusp forms.

For an arbitrary deformation, we present a general numerical procedure, based on the collocation method, which enables one to calculate the complex resonance energy eigenvalues. We thus follow the transition in the distributions of the positions of the resonances and their widths as we deform the boundary away from the arithmetic Artin's billiard. Initially, the width distribution is shown to evolve into a chi-squared distribution, but then as one approaches the arithmetic $n = 4$ Hecke billiard, it splits into three distinct groups of resonances: one which moves closer to the real axis, another which forms the resonances given by the zeros of the Riemann zeta function and a third group which have their positions at equal spacings determined by the width of the billiard. As the boundary is further varied away from the

$n = 4$ case, a chi-squared distribution is again recovered and the pattern is repeated as the next arithmetical case is encountered for $n = 6$. The distribution of the positions of the resonances also evolves and is shown to be consistent with the predictions of the RMT for non-arithmetical cases including the Hecke triangular billiard for $n = 5$.

The billiard system and the deformation considered are introduced in section 2. The derivation of the scattering matrix for the Hecke triangular billiards, $n = 4$ and 6, is given in section 3 and the methods involved in the calculation of the resonances in the general case are outlined in section 4. The statistics of the resonances are investigated in section 5 and conclusions are reserved for section 6.

2. Hecke groups and the parameterization of the transition between their corresponding billiard systems

The Poincaré half-plane is the upper-half of the complex plane in a space with constant negative curvature (for a review, see [11]). In this model of hyperbolic geometry, the coordinates are endowed with a metric

$$g_{ij} = y^{-2}\delta_{ij}. \tag{1}$$

The geodesics in this geometry are circles centred on the x-axis. We will use the fundamental domains of discrete groups in this geometry as our open billiard systems. The groups we focus on are the Hecke groups $\Gamma(2, n)$ for the Poincaré half-plane, $\mathbb{H}$, which are generated by the two matrices or transformations S and T,

$$S = \begin{pmatrix} 0 & -1 \\ 1 & 0 \end{pmatrix}, \qquad T = \begin{pmatrix} 1 & \mathcal{L} \\ 0 & 1 \end{pmatrix}, \tag{2}$$

where

$$\mathcal{L} = 2\cos(\pi/n), \qquad n \in \mathbb{Z} | n > 2. \tag{3}$$

Elements of $\Gamma(2, n)$ act on points of the half plane with the coordinates x and y defined as

$$x = \mathrm{Re}(z), \qquad y = \mathrm{Im}(z); \qquad z = x + \imath y, \tag{4}$$

such that

$$\Gamma(z) = \frac{az + b}{cz + d}, \qquad \Gamma = \begin{pmatrix} a & b \\ c & d \end{pmatrix} \in \Gamma(2, n), \tag{5}$$

where a, b, c and d are real numbers in general with $ad - bc = 1$. This is a fractional linear transformation or Möbius transformation which preserves the hyperbolic distance between any two points in the plane. In these coordinates, S and T correspond to the operations of inversion in the unit circle and translation in x by the distance $\mathcal{L}$, respectively [4].

Using S and T, it is easy to show that a fundamental domain for each group can be taken as the region in $\mathbb{H}$ defined by

$$|\mathrm{Re}(z)| \leqslant \mathcal{L}/2, \qquad |z| \geqslant 1, \quad z \in \mathbb{H}. \tag{6}$$

In figure 1, the fundamental domains for the Hecke groups correspond to $\mathcal{L}/2 = \cos(\pi/n) = \cos(\theta)$, $n \in \mathbb{Z} | n > 2$ and hence correspond to specific lengths $\mathcal{L}$ and angles θ. (Note that the 'triangle' shape is more clearly seen in the Poincaré disk representation of hyperbolic space. In figure 1, the angles of the triangle are θ, $\pi/2$ and 0 at infinity.) The half plane is tiled by copies of the fundamental domain generated by S and T.

Figure 1 also illustrates the general open billiard we wish to consider for an arbitrary $\mathcal{L}$. The y-axis is clearly a symmetry axis and when we study the Schrödinger equation (or

equivalently the Laplace–Beltrami operator), we can classify the solutions as being even or odd with respect to reflection about this axis. It is easy to show that for odd states this is equivalent to taking Dirichlet boundary conditions on all of the walls in billiard A and generates a discrete spectrum only. For even states, we have instead Neumann boundary conditions on all the walls in A. It is the even class which contains the continuum and the resonances and it is those which are of interest in this paper, so our results are confined to one symmetry class of the spectrum of the full group. Several studies have been done on bound spectra for this and other symmetry classes, for instance in [11, 12].

The behaviour of the quantum spectrum can be followed as $\mathcal{L}$ varies continuously in the range $1 \leqslant \mathcal{L} < 2$. The case $\mathcal{L} = 1$ corresponds to the modular group and as $\mathcal{L}$ is changed as seen above we encounter each of the Hecke triangle groups $\Gamma(2, n)$ in sequential order of increasing n. The system is open at $y = \infty$ for all values of $\mathcal{L}$ and, classically, the particles are allowed to enter or leave via this *cusp* (a cusp is a corner with an angle zero). The restricted nature of the scattering from these billiards will mean that there is only one available channel for the quantum scattering, which greatly simplifies matters when compared with general open systems (see section 3).

By keeping the lower boundary fixed on the unit circle centred at the origin, we ensure all the walls are geodetic, and thus they provide no focusing or defocusing of trajectories. The classical dynamics are ergodic for the whole parameter range in $\mathcal{L}$ and this is due solely to the exponential divergence of trajectories caused by the negative curvature of the Poincaré half-plane. The generic behaviour for chaotic systems is thus expected in the cases where $\mathcal{L}$ does not happen to be the region of a fundamental domain of an arithmetic Hecke group [4].

In fact, one might expect non-generic behaviour for all the cases where there is a group underlying the triangle ($\theta = \pi/n$) but it has been shown [13] that similar behaviour to that in Artin's billiard is only found for the arithmetic cases $n \in \{3, 4, 6\}$ (that is, not at $n = 5$, which is the other case studied here). In these cases, $\mathcal{L}^2$ is an integer and the matrix elements of the group can be expressed simply. In general, they belong to the broader class of arithmetic groups where the trace of the matrix representations are algebraic integers. The Hecke groups are particularly simple examples. These features also enable one to construct an explicit expression for the scattering matrix, S, for the arithmetic cases.

3. Quantum scattering for discrete groups

Since the metric in the Poincaré half-plane is (1), $g_{ij} = y^{-2}\delta_{ij}$, the Schrödinger equation for these billiards is [11]

$$y^2\left(\frac{\partial^2}{\partial x^2} + \frac{\partial^2}{\partial y^2}\right)\psi = -\lambda\psi, \tag{7}$$

where $\lambda = 2mE/\hbar^2 + \frac{1}{4}$ and E is the energy of a particle of mass m.

The systems under consideration were described in section 2 and were illustrated in figure 1. The deformation shifts the right-hand vertical wall, while keeping the lower boundary fixed as the unit circle in the half plane. Solutions of (7) are sought which obey Neumann boundary conditions on all walls. Considering first this boundary condition on $x = 0$ and $x = \mathcal{L}/2$, that is

$$\frac{\partial\psi}{\partial\hat{n}} = 0, \tag{8}$$

where $\frac{\partial}{\partial \hat{n}}$ is the normal derivative of the wavefunction on the boundary, by separation of variables one can write an infinite set of solutions to (7) for fixed λ that satisfy this condition in the form

$$\psi_m(k; x, y) = \cos(2\pi m x/\mathcal{L}) f_m(y), \tag{9}$$

where m is an integer. On substitution into (7), we obtain the Bessel equation for $f_m(y)$,

$$\frac{\mathrm{d}^2 f_m}{\mathrm{d}y^2} + \left[\frac{k^2 + 1/4}{y^2} - \left(\frac{2m\pi}{\mathcal{L}}\right)^2\right] f_m = 0, \tag{10}$$

where $k = \sqrt{2mE}/\hbar$ is the scaled momentum. For $m \neq 0$ the bounded solutions as $y \to \infty$ are $f_m = \sqrt{y} K_{\imath k}(2\pi m y/\mathcal{L})$, where $K_{\imath k}$ is the modified Bessel function of imaginary order and $K_{\imath k}$ decay exponentially as $y \to \infty$. For $m = 0$ the solutions are $y^{1/2 \pm \imath k}$. Hence, for $m = 0$ a general continuum solution is of the form

$$\psi_0(k; y) = y^{1/2}(y^{-\imath k} + S(k) y^{\imath k}). \tag{11}$$

This solution represents incoming and outgoing waves at infinity. S is the S-matrix, here a scalar since there is only one open or scattering channel available as mentioned earlier in section 2. Together with the bounded solutions (9), this forms a complete set of solutions to the scattering problem.

To satisfy the final boundary condition (8) on the lower boundary in figure 1, we take a linear combination of the decaying and continuum wavefunctions at a given energy. This will thus have the form

$$\psi(k; x, y) = b_0 y^{1/2}(y^{-\imath k} + S(k) y^{\imath k}) + \sum_{m=1}^{\infty} b_m(k) \cos(2\pi m x/\mathcal{L}) \sqrt{y} K_{\imath k}(2\pi m y/\mathcal{L}). \tag{12}$$

This is essentially a Fourier decomposition of the solution. Due to the unusual nature of these scattering systems, conventional techniques for locating resonances proved troublesome and instead a modified collocation method was used for the numerical solution of (7), following its successful application in [14]. Before giving the details of this method, we show that for the special cases of $\mathcal{L} = \sqrt{2}$ and $\mathcal{L} = \sqrt{3}$, $S(k)$ can be obtained analytically. In the mathematics literature, formal expressions have been given for the scattering matrix for a general discrete group [15]. We derive below the explicit expressions for the scattering matrix for the arithmetic cases $n = 4$ and 6. A detailed presentation of the calculation for the S matrix, for the modular group the $n = 3$ case, can be found in, e.g., [16–18].

3.1. The scattering matrix for $\mathcal{L} = \sqrt{2}$

For this case $n = 4$ in (3) and the group is generated by the specific matrices

$$S = \begin{pmatrix} 0 & -1 \\ 1 & 0 \end{pmatrix}, \qquad T = \begin{pmatrix} 1 & \sqrt{2} \\ 0 & 1 \end{pmatrix}. \tag{13}$$

Thus, the matrix representations of particular group elements take two forms:

$$\sigma = \begin{pmatrix} a & b \\ c & d \end{pmatrix} = \begin{pmatrix} 1 + 2a' & b'\sqrt{2} \\ c'\sqrt{2} & 1 + 2d' \end{pmatrix}; \{a', b', c', d' \in \mathbb{Z} | ad - 2b'c' = 1\} \tag{14}$$

and

$$\sigma = \begin{pmatrix} a & b \\ c & d \end{pmatrix} = \begin{pmatrix} a'\sqrt{2} & 1 + 2b' \\ 1 + 2c' & d'\sqrt{2} \end{pmatrix}; \{a', b', c', d' \in \mathbb{Z} | 2a'd' - bc = 1\}. \tag{15}$$

Following Gutzwiller's derivation [17], we sum the image of an incoming free plane wave $y^{1/2-\imath k}$ over all images of the fundamental domain of the group $\Gamma(2,4)$.

We thus obtain a general expression for the scattered wavefunction

$$\psi(x,y)=\psi(z)=\sum_{\sigma\in\Gamma(2,4)}\frac{y^{1/2-\imath k}}{|cz+d|^{1-2\imath k}}, \tag{16}$$

where only unique images under the mapping σ are summed over.

The symmetry of this sum enforces the desired periodic boundary conditions on ψ since

$$\psi(x,y)=\psi(z)=\psi(\sigma(z)) \tag{17}$$

by construction. It is also obviously a solution to the Schrödinger equation (7) since the Laplacian commutes with all the mappings $g_\sigma = z\mapsto\sigma(z)$. This technique of enforcing boundary conditions by linearly superposing solutions to a differential equation is familiar to physicists as the method of images. It is equivalent to the intuitive method of multiple scattering used, for example in [19], to calculate the resonance spectrum of a three-disc scattering system.

Starting from (16) and considering which group elements to include in the sum, we first factor out the left coset Γ_0 since

$$\Gamma_0=\left\{\begin{pmatrix}1 & q\sqrt{2}\\ 0 & 1\end{pmatrix}\right\};q\in\mathbb{Z} \tag{18}$$

and thus

$$\Gamma_0\sigma=\left\{\begin{pmatrix}a+q\sqrt{2}c & b+q\sqrt{2}d\\ c & d\end{pmatrix}\right\}, \tag{19}$$

which all produce the same $y(\sigma z)=y/|cz+d|^2$.

Next we consider the Fourier decomposition $\psi=\sum_m a_m(y)\exp(-2\pi\imath mx/\mathcal{L})$. ψ for this group is periodic with period $\sqrt{2}$ in x so concentrating on a_0 which leads to the S matrix as can be seen from equation (12), we get

$$a_0(y)=\frac{1}{\sqrt{2}}\int_0^{\sqrt{2}}\sum_{\sigma\in\Gamma_0\backslash\Gamma(2,4)}\frac{y^{1/2-\imath k}}{|cz+d|^{1-2\imath k}}\mathrm{d}x. \tag{20}$$

The identity term in the sum ($c=0,d=1$) gives a contribution $y^{1/2-\imath k}$ and there are two cases to consider when treating the right cosets

$$\sigma\Gamma_0=\left\{\begin{pmatrix}a & b+q\sqrt{2}a\\ c & d+q\sqrt{2}c\end{pmatrix}\right\}. \tag{21}$$

These are equal only for any σ and $\tilde{\sigma}$ with $\tilde{c}=c$ and $\tilde{d}\equiv d(\mathrm{mod}\sqrt{2}c)$. In both cases, only one coset representative is required in the sum and the rest are taken into the integral via

$$y(\sigma z)=\frac{y}{|cz+d+q\sqrt{2}c|^2}=\frac{y}{|c(z+q\sqrt{2})+d|^2}, \tag{22}$$

so that

$$\int_0^{\sqrt{2}}y(\sigma(z))^{1/2-\imath k}\,\mathrm{d}x=\int_{q\sqrt{2}}^{(q+1)\sqrt{2}}y(z')^{1/2-\imath k}\,\mathrm{d}x' \tag{23}$$

by the simple substitution $x'=x+q\sqrt{2}$.

This brings us to a point where (20) can be written as

$$a_0(y) = y^{1/2-\imath k} + \frac{1}{\sqrt{2}} \int_{-\infty}^{\infty} \sum_{\sigma \in \Gamma_0 \backslash \Gamma(2,4)/\,\Gamma_0 - \mathbb{I}} \frac{y^{1/2-\imath k}}{|cz+d|^{1-2\imath k}}\, \mathrm{d}x. \tag{24}$$

Substituting $\rho = x + d/c$, this becomes

$$a_0(y) = y^{1/2-\imath k} + \frac{1}{\sqrt{2}} \sum_{\sigma \in \Gamma_0 \backslash \Gamma(2,4)/\,\Gamma_0 - \mathbb{I}} \frac{1}{|c|^{1-2\imath k}} \int_{-\infty}^{\infty} \frac{y^{1/2-\imath k}}{(\rho^2+y^2)^{1/2-\imath k}}\, \mathrm{d}\rho. \tag{25}$$

In the first case considered above, equation (14), the $\sqrt{2}$ factor is contained in c and the determinant constraint $ad - 2b'c' = 1$ means that c' is coprime to d since ad is odd. Thus, we have to sum over all

$$c = \sqrt{2}c', \qquad c' \in \mathbb{Z} \tag{26}$$

and the sum over d is over all odd integers less than $2c'$ and coprime to c'. Since $2c'$ is even, this is just $\phi(2c')$, the number of integers less than $2c'$ and coprime to $2c'$.

In the second case, equation (15), $\sqrt{2}$ is contained in d so we have to sum over all *odd* integers c, and the sum over d ranges over all integers d' that are less than c. Thus, we get a contribution $\phi(c)$ from the sum over d, since the determinant constraint $2a'd' - bc = 1$ now means that d' is coprime to c (bc is odd).

Equation (25) now reads

$$a_0(y) = y^{1/2-\imath k} + \frac{1}{\sqrt{2}} \int_{-\infty}^{\infty} \frac{y^{1/2-\imath k}}{(\rho^2+y^2)^{1/2-\imath k}}\, \mathrm{d}\rho \left(\sum_{0<c'\in\mathbb{Z}} \frac{\phi(2c')}{2^{1/2-\imath k} c'^{(1-2\imath k)}} + \sum_{0\leqslant c'\in\mathbb{Z}} \frac{\phi(1+2c')}{(1+2c')^{1-2\imath k}} \right). \tag{27}$$

So we have two sums to consider and the total arithmetic term in (27) becomes (putting $s = 1/2 - \imath k$ and substituting c for c' as the dummy index)

$$\sum_{c\ \mathrm{odd}} \frac{\phi(c)}{c^{2s}} + 2^s \sum_{c\ \mathrm{even}} \frac{\phi(c)}{c^{2s}}. \tag{28}$$

Expanding the sums via the unique representation of integers by primes (cf the Euler product form for the Riemann zeta function—see [20] for this and many other useful identities), then factoring out all terms containing factors of 2, we obtain for the sum over odd integers

$$\begin{aligned} \sum_{c} \frac{\phi(c)}{c^{2s}} &= \prod_{p} \left\{ 1 + \frac{\left(1-\frac{1}{p}\right)}{p^{(2s-1)}} \left(1 + \frac{1}{p^{(s-1)}} + \cdots \right) \right\} \\ &= \prod_{p} \left\{ \frac{\left(1-\frac{1}{p^{(2s-1)}}\right) + \left(\frac{1}{p^{(2s-1)}} - \frac{1}{p^{2s}}\right)}{\left(1-\frac{1}{p^{(2s-1)}}\right)} \right\} \\ &\Rightarrow \sum_{c\ \mathrm{odd}} \frac{\phi(c)}{c^{2s}} = \frac{(1-1/2^{(2s-1)})\zeta(2s-1)}{(1-1/2^{2s})\zeta(2s)}, \end{aligned} \tag{29}$$

and the even sum can then simply be written as

$$\sum_{c\ \mathrm{even}} \frac{\phi(c)}{c^{2s}} = \frac{\zeta(2s-1)}{\zeta(2s)} \left(1 - \frac{(1-1/2^{(2s-1)})}{(1-1/2^{2s})} \right) = \frac{\zeta(2s-1)}{\zeta(2s)(2^{2s}-1)}. \tag{30}$$

Putting all this together finally gives

$$\sum_{c\ \mathrm{odd}} \frac{\phi(c)}{c^{2s}} + 2^s \sum_{c\ \mathrm{even}} \frac{\phi(c)}{c^{2s}} = \frac{\zeta(2s-1)}{\zeta(2s)} \frac{(2+2^s)}{(1+2^s)}, \tag{31}$$

The integral in (27) can be transformed to a representation of the beta function [21],

$$\int_{-\infty}^{\infty} \frac{y^{1/2-\imath k}}{(\rho^2+y^2)^{1/2-\imath k}}\mathrm{d}\rho = y^{1-(1/2-\imath k)}\frac{\Gamma(1/2)\Gamma(-\imath k)}{\Gamma(1/2-\imath k)}. \tag{32}$$

Then using the functional equation for the zeta function

$$Z(w) = \pi^{-w/2}\Gamma(w/2)\zeta(w) = Z(1-w), \tag{33}$$

we obtain a final expression for the S matrix (resubstituting $s = 1/2 - \imath k$ and remembering the factor $1/\sqrt{2}$ from (27))

$$S(k) = 2^{\imath k}\frac{(\sqrt{2}+2^{-\imath k})}{(\sqrt{2}+2^{\imath k})}\frac{\pi^{-\imath k}\Gamma(1/2+\imath k)\zeta(1+2\imath k)}{\pi^{\imath k}\Gamma(1/2-\imath k)\zeta(1-2\imath k)}, \tag{34}$$

where ζ is Riemann's zeta function and Γ is Euler's gamma function. S therefore has poles on the line $\mathrm{Im}(k) = -1/4$, positioned at the non-trivial zeros of the Riemann zeta function divided by 2 as in the modular case for $n = 3$, but also in addition a set of regular equally spaced resonances at

$$k = r - \imath/2, \qquad r = (1+2n)\pi/(\ln 2), \qquad n \in \mathbb{Z}. \tag{35}$$

The Fourier coefficients $a_m(y)$ for general m are calculated in the appendix.

3.2. The scattering matrix for $\mathcal{L} = \sqrt{3}$

In this case $n = 6$ in (3) and the group is generated by the specific matrices

$$S = \begin{pmatrix} 0 & -1 \\ 1 & 0 \end{pmatrix}, \qquad T = \begin{pmatrix} 1 & \sqrt{3} \\ 0 & 1 \end{pmatrix}. \tag{36}$$

Thus, the matrix representations of particular group elements now take four forms:

$$\sigma = \begin{pmatrix} a & b \\ c & d \end{pmatrix} = \begin{pmatrix} 1+3a' & b'\sqrt{3} \\ c'\sqrt{3} & 1+3d' \end{pmatrix} \quad \text{or} \quad \begin{pmatrix} 2+3a' & b'\sqrt{3} \\ c'\sqrt{3} & 2+3d' \end{pmatrix};$$
$$\{a', b', c', d' \in \mathbb{Z} | ad - 3b'c' = 1\} \tag{37}$$

and

$$\sigma = \begin{pmatrix} a & b \\ c & d \end{pmatrix} = \begin{pmatrix} a'\sqrt{3} & 2+3b' \\ 1+3c' & d'\sqrt{3} \end{pmatrix} \quad \text{or} \quad \begin{pmatrix} a'\sqrt{3} & 1+3b' \\ 2+3c' & d'\sqrt{3} \end{pmatrix};$$
$$\{a', b, c, d' \in \mathbb{Z} | 3a'd' - bc = 1\}. \tag{38}$$

The task of calculating the scattering coefficient proceeds almost exactly as in section 3.1 for the case $n = 4$. Taking a Fourier decomposition of (16) with period $\sqrt{3}$ and factoring out the left cosets brings us to an expression for the constant Fourier coefficient,

$$a_0(y) = y^{1/2-\imath k} + \frac{1}{\sqrt{3}}\sum_{\sigma\in\Gamma_0\backslash\Gamma(2,6)/\Gamma_0-\mathbb{I}} \frac{1}{|c|^{1-2\imath k}}\int_{-\infty}^{\infty}\frac{y^{1/2-\imath k}}{(\rho^2+y^2)^{1/2-\imath k}}\,\mathrm{d}\rho. \tag{39}$$

The sum naturally splits into two parts over the two classes of matrices described in (37) and (38),

$$a_0(y) = y^{1/2-\imath k} + \frac{1}{\sqrt{3}}\int_{-\infty}^{\infty}\frac{y^{1/2-\imath k}}{(\rho^2+y^2)^{1/2-\imath k}}\,\mathrm{d}\rho\left(\sum_{0<c\in\mathbb{Z}}\frac{3^{1/2-\imath k}\phi(3c)}{(3c)^{1-2\imath k}} + \sum_{0<c\in\mathbb{Z}|(c,3)=1}\frac{\phi(c)}{(c)^{1-2\imath k}}\right). \tag{40}$$

Performing these sums as done earlier for the case $\mathcal{L} = \sqrt{2}$ in (29), the expression for the scattering coefficient reduces to $\frac{\zeta(2s-1)}{\zeta(2s)}$ times the unitary factor

$$3^{\imath k}\frac{(\sqrt{3}+3^{-\imath k})}{(\sqrt{3}+3^{\imath k})}; \tag{41}$$

thus,

$$S(k) = 3^{\imath k}\frac{(\sqrt{3}+3^{-\imath k})}{(\sqrt{3}+3^{\imath k})}\frac{\pi^{-\imath k}\Gamma(1/2+\imath k)\zeta(1+2\imath k)}{\pi^{\imath k}\Gamma(1/2-\imath k)\zeta(1-2\imath k)}, \tag{42}$$

which has poles on the line $\mathrm{Im}(k) = -1/4$, positioned at the non-trivial zeros of the Riemann zeta function divided by 2, and in addition a set of regularly spaced resonances at

$$k = r - \imath/2, \qquad r = (1+2n)\pi/(\ln 3), \qquad n \in \mathbb{Z}. \tag{43}$$

4. Expansion method for locating resonances at an arbitrary $\mathcal{L}$

Outside of the three special cases for $n = 3$, 4 and 6, it is not possible to calculate analytically the S-matrix and the resonance positions. To obtain large numbers of resonances, which are necessary for performing a statistical analysis of the spectra, a method was developed which has proved useful over a wide momentum and deformation parameter range $\mathcal{L}$. In essence, it involves calculating the Fourier coefficients in an expansion of the type (equation (12)) but using the boundary conditions appropriate to resonance wavefunctions.

When considering an expansion of a resonance wavefunction into a basis set of the form (12), in order to directly calculate the resonance energies one must enforce the outgoing wave boundary condition at infinity. That is, we require $\lim_{y\to\infty}\psi(k;x,y) = y^{1/2+\imath k}$, an outgoing wave only. To do this, we replace the continuum wavefunction by $\psi_0(k;x,y) = y^{1/2+\imath k}$ instead of the form given in (11). The full wavefunction is thus expanded in the form

$$\Psi_N(k;x,y) = \sum_{m=0}^{N-1} A_m\psi_m(k;x,y), \tag{44}$$

where $\psi_m(k;x,y)$ were defined in equation (9) for $m \neq 0$ and given above for $m = 0$.

This wavefunction by construction represents a resonance state and obeys the Neumann boundary condition at $x = 0$ and $x = \mathcal{L}/2$. To determine the coefficients A_m and the complex resonance eigenenergies or eigenmomenta k, one must enforce the Neumann boundary condition on the lower boundary in figure 1. Here this is done by using a modified collocation method [22, 23].

One calculates the normal derivative of (44) on the lower boundary and Fourier expands it into a set of N orthogonal functions $\sin\left(\frac{n\pi s}{L}\right)$. As discussed in, e.g. [22, 24], this modification of the method has several advantages. The first N Fourier coefficients of this expansion D_n are given by

$$D_n = \sum_{m=0}^{N-1} C_{nm}A_m, \tag{45}$$

where

$$C_{nm} = \oint \mathrm{d}s \sin\left(\frac{n\pi s}{L}\right)\frac{\partial\psi_m}{\partial\hat{n}}(k;s), \qquad n = 1,\ldots,N; \tag{46}$$

s is a parameterization of the lower billiard boundary and L is its length in that parameterization. In (46), s ranges from 0 to

$$s_{\max} = 2\tanh^{-1}\left(\sqrt{\frac{(\mathcal{L}/2)^2 + (1-\sqrt{1-(\mathcal{L}/2)^2})^2}{(\mathcal{L}/2)^2 + (1+\sqrt{1-(\mathcal{L}/2)^2})^2}}\right), \tag{47}$$

where the geodesic distance is used. The normal derivative on the lower boundary is given by

$$\frac{\partial}{\partial \hat{n}}(\psi_m) = \underline{\nabla}\psi_m \cdot \underline{\hat{n}} = yx\frac{\partial \psi_m}{\partial x} + y^2\frac{\partial \psi_m}{\partial y}. \tag{48}$$

The final ingredient in calculating the matrix elements (46) is the integral over s, for which an extended tenth-order quadrature formula is used.

The boundary condition on the lower boundary is now satisfied by setting the Fourier coefficients (45) equal to zero or equivalently by searching for the complex values k such that the determinant of the N by N complex matrix C_{nm} is zero. The summations are necessarily truncated at N, but N is chosen sufficiently large to achieve convergence of the eigenvalues. The higher the energy of the resonance, the more values of n and m are required. We scale N with the momentum so that $N = \mathrm{int}(r_{\mathrm{scal}} + \alpha)$, where

$$r_{\mathrm{scal}} = \mathrm{Re}(k)\mathcal{L}/(2\pi\sqrt{1-(\mathcal{L}/2)^2}) \tag{49}$$

and int means taking the integer part of the expression. α is a small integer (good convergence was achieved for values of α between 2 and 6) which can be varied to help convergence for particular resonances. For higher values of N, the Bessel functions included become exponentially small and do not contribute significantly. This is due to the turning point in the differential equation (10) at $k \approx 2\pi m y/\mathcal{L}$. Conservatively, setting y to its lowest point in the billiard gives the scaling (49). In fact this is excessive and the parameter α can be lowered at large $\mathcal{L}$ to compensate.

In order to avoid overflowing the maximum computational precision available, each row of the matrix is scaled by its largest element, that is

$$C_{nm} \to C_{nm}/(\max_n(C_{nm})), \tag{50}$$

$\max_n$ indicating the maximum value of the operand when n takes all possible values. Then, a singular-value decomposition is performed, using a standard LAPACK routine, to ease detection of the complex zeros of the determinant [25, 26].

The most time-consuming part of our routine, aside from the iterations required to reach any desired value of the perturbation parameter, is the setting up of the matrix (46) due to the many calculations of the Bessel functions (here involving complex values of k) required for each element. Powerful expansions similar to those in [23] are used taken mostly from [27] but largely based on routines used in [28].

In order to calculate the widths and positions of the resonances at new values of the deformation parameters, first many eigenvalues, both cusp forms and resonances, were obtained for the modular group ($\mathcal{L} = 1$), details of which were given in [14]. Using these values as seeds for the calculation, the parameter $\mathcal{L}$ can be varied a little, and a search in the complex plane for zeros of the least singular value of the matrix $\mathbf{C}$ near to the old values is performed. Then the parameters can be varied again, by larger amounts at each step, as information about the velocity of each resonance with each parameter allows better guesses as to the perturbed value.

The main case where there are results available [29–31] to check against those obtained here is for Artin's billiard ($\mathcal{L} = 1$). The S-matrix for $\mathcal{L} = 1$ is

$$S(k) = \frac{\pi^{-\imath k}\Gamma\left(\frac{1}{2}+\imath k\right)\zeta(1+2\imath k)}{\pi^{\imath k}\Gamma\left(\frac{1}{2}-\imath k\right)\zeta(1-2\imath k)}, \tag{51}$$

Table 1. Comparison of methods for finding resonances of the billiard systems for the arithmetical cases, where m is just used to sequentially label the resonances.

m, $\mathcal{L}$	Exact	Expansion method
2, 1	10.511 020 $-0.25\imath$	10.511 125 $-0.250\,008\imath$
4, 1	13.779 751 $-0\imath$	13.779 625 $0.000\,005\imath$
10, 1	20.459 360 $-0.25\imath$	20.459 875 $-0.250\,315\imath$
50, 1	40.688 666 $-0\imath$	40.688 500 $-0.000\,000\imath$
200, 1	76.512 345 $-0.25\imath$	76.512 346 $-0.250\,000\imath$
1, $\sqrt{2}$	4.532 360 $-0.5\imath$	4.532 432 $-0.499\,993\imath$
4, $\sqrt{2}$	10.511 020 $-0.25\imath$	10.511 002 $-0.249\,965\imath$
10, $\sqrt{2}$	15.212 438 $-0.25\imath$	15.212 431 $-0.250\,022\imath$
25, $\sqrt{2}$	24.112 353 $-0\imath$	24.112 326 $0.000\,040\imath$
1, $\sqrt{3}$	2.859 601 $-0.5\imath$	2.859 602 $-0.500\,005\imath$
4, $\sqrt{3}$	8.038 861 $-0\imath$	8.038 862 $0.000\,000\imath$
10, $\sqrt{3}$	12.505 428 $-0.25\imath$	12.505 423 $-0.249\,999\imath$
25, $\sqrt{3}$	19.896 104 $-0\imath$	19.896 104 $-0.000\,000\imath$

where $\Gamma(z)$ is Euler's gamma function and $\zeta(z)$ is Riemann's zeta function [7, 32]. The resonances (poles of S) are given by the zeros of the denominator, which occur at $k = k_n/2 - \imath/4$, according to the Riemann hypothesis, where k_n are the tabulated Riemann zeros. (The 'trivial' zeros of $\zeta(1 - 2\imath k)$ are cancelled by the zeros of $\Gamma(\frac{1}{2} + \imath k)$ except for $k = \imath/2$ which gives the single bound state at $k^2 = -1/4$.) Many tabulated eigenvalues also exist for the even cusp forms for $\mathcal{L} = 1$ and a more restricted set for $\mathcal{L} = \sqrt{2}$ and $\mathcal{L} = \sqrt{3}$ [12]. The numerical results presented here give both the resonances on the critical line and the cusp forms in one calculation. This method produces results in agreement with the cusp forms found in the literature [12, 29–31] for the known cases of $\mathcal{L} \in \{1, \sqrt{2}, \sqrt{3}\}$.

Table 1 gives some of our results for the resonance spectra of the billiard systems parameterized by $\mathcal{L}$. The title 'exact' for the first column refers to tabulated results for the Riemann zeros, numerical results for the cusp forms calculated by other groups [30, 12, 31], and predictions from equations (35) and (43) accurate to at least five decimal places. In our calculations using the expansion method, we worked to the fourth decimal place and one can see that good agreement is obtained at this level.

In the following sections, we present our results for the distribution of resonances for a general deformation length $\mathcal{L}$ starting from the case of Artin's billiard and deforming the right-hand wall continuously until $\mathcal{L} = \sqrt{3}$ is reached, which is the point where our present calculations were terminated, all arithmetic systems having been covered.

5. Results

5.1. The widths

We first show the distributions for the imaginary parts of the resonance positions or the widths. Figures 2–8 show the numerical integrated width density $I(w)$ as it evolves in the range $1.000 \leqslant \mathcal{L} \leqslant \sqrt{3}$. RMT predicts a Porter–Thomas distribution for the widths for generic single-channel chaotic scattering systems [8]. The dashed curve is the integrated Porter–Thomas distribution given by

$$I(w) = \mathrm{erf}(\sqrt{w_n/2}), \tag{52}$$

where $\mathrm{erf}(x)$ is the error function and w_n is the resonance width normalized to its mean value.

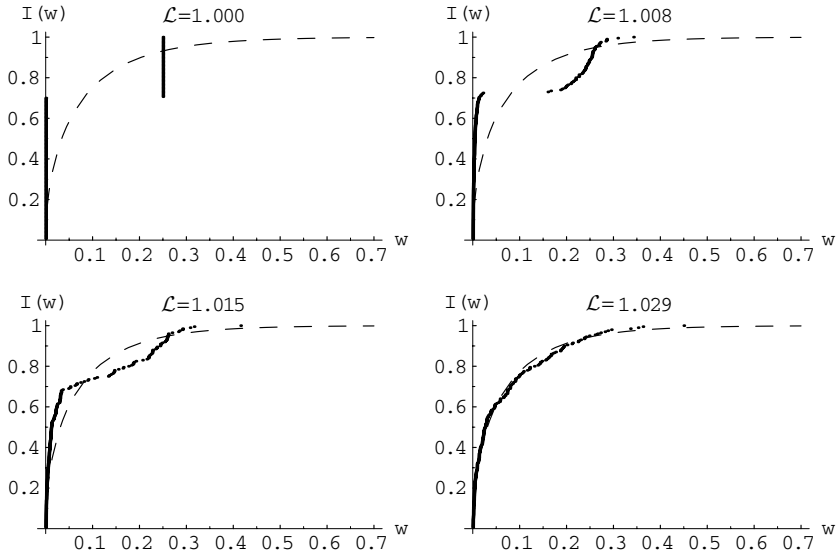

Figure 2. Integrated width density of 200 resonances for $\mathcal{L}$ between 1.000 and 1.029. The dashed curve is the integrated Porter–Thomas distribution. The case $\mathcal{L} = 1.000$ corresponds to the Hecke group (Artin's billiard) with $\theta = \pi/3$.

Figures 2, 6 and 8 show the transition to arithmetic chaos near the special cases of arithmetic groups at $\mathcal{L} = \sqrt{1}, \sqrt{2}$ and $\sqrt{3}$, corresponding to $\theta = \pi/3, \pi/4$ and $\pi/6$, respectively. In these cases, we see the predictions of sections 3.1 and 3.2 confirmed in the numerical work with the existence of a class of resonance states with imaginary part equal to $-\frac{1}{4}$ positioned at the Riemann zeros, i.e. $k = k_n/2 - \imath/4$, as in the case of the modular domain, and a class with imaginary part equal to $-\frac{1}{2}$ positioned at regular intervals of $\frac{2\pi}{\ln(\mathcal{L})}$.

The width distribution clearly does not follow the Porter–Thomas distribution at or near to these three special arithmetic cases but as $\mathcal{L}$ is varied away from these particular cases, the three groups of 'resonances' merge again and the distribution becomes much closer to the generic Porter–Thomas distribution (see figures 4 and 7). There appears to be no significant correlation between which states fall into which class at different values of $\mathcal{L}$, in fact states often switch class during the intermediate deformation. The phenomenon seen here is attributed purely to arithmetic chaos due to the underlying groups' structure. The best agreement with RMT appears to be for $\mathcal{L} = 1.252$. For other $\mathcal{L}$, away from the arithmetical cases, there seems to be a reasonable agreement with RMT. However, one would need a larger set of resonances to make a more definitive statement about the statistics. In figure 7, the case $\mathcal{L} = 1.618, \theta = \pi/5$ corresponds to the Hecke group with $n = 5$ and the distribution is clearly different from the $n = 3, 4$ and 6 cases and it is seen to agree reasonably well with the generic RMT case, although there is some discrepancy for shorter widths. Bogomolny and Schmit [33] have shown that there are exponential degeneracies for the periodic orbits for this case also although with a lower exponent than for the arithmetic cases. This may be true for intermediate $\mathcal{L}$ also and may have an effect on the distributions.

A perhaps surprising aspect of the widths for arithmetic cases $n = 4$ and $n = 6$ from the quantum chaos perspective is the appearance of a set of regularly spaced resonances related to the width of the billiard which would give rise to regular modulations in the time delay [32]. This is reminiscent of the regular modulations in the density of states for the stadium billiard

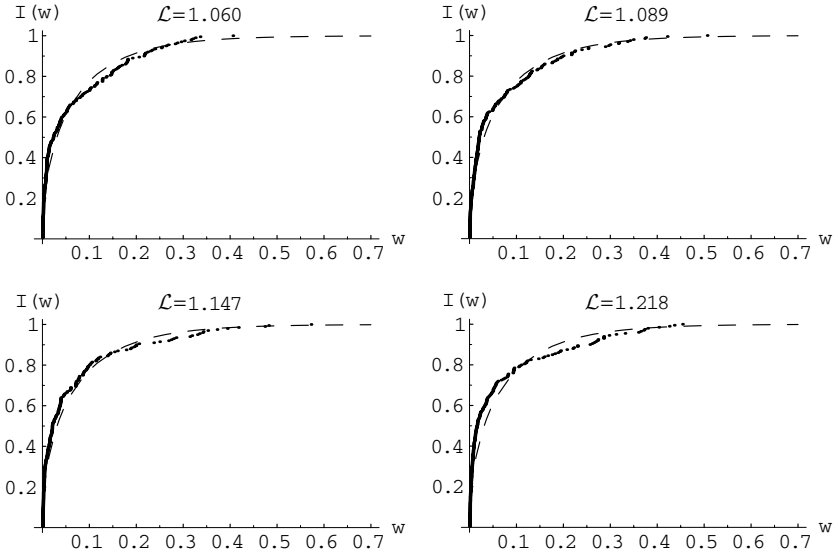

Figure 3. Integrated width density of 200 resonances for $\mathcal{L}$ between 1.060 and 1.218. The dashed curve is the integrated Porter–Thomas distribution.

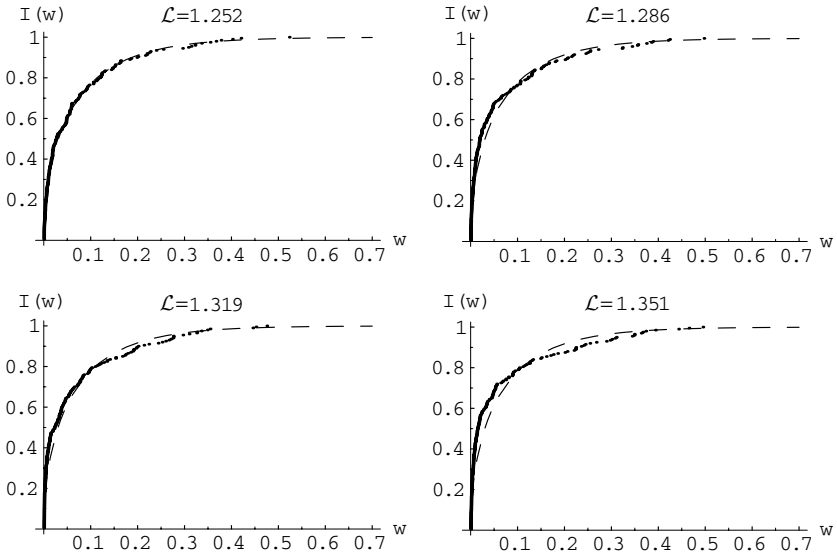

Figure 4. Integrated width density of 200 resonances for $\mathcal{L}$ between 1.252 and 1.351. The dashed curve is the integrated Porter–Thomas distribution.

due to the family of 'bouncing ball' orbits [34, 25] although no such family would appear to exist for arithmetic hyperbolic systems .

5.2. Level-spacing statistics

The nearest-neighbour distribution for the statistics of the unfolded eigenmomenta is shown in figures 9–11. The distributions of level-spacings include the three arithmetic cases, and

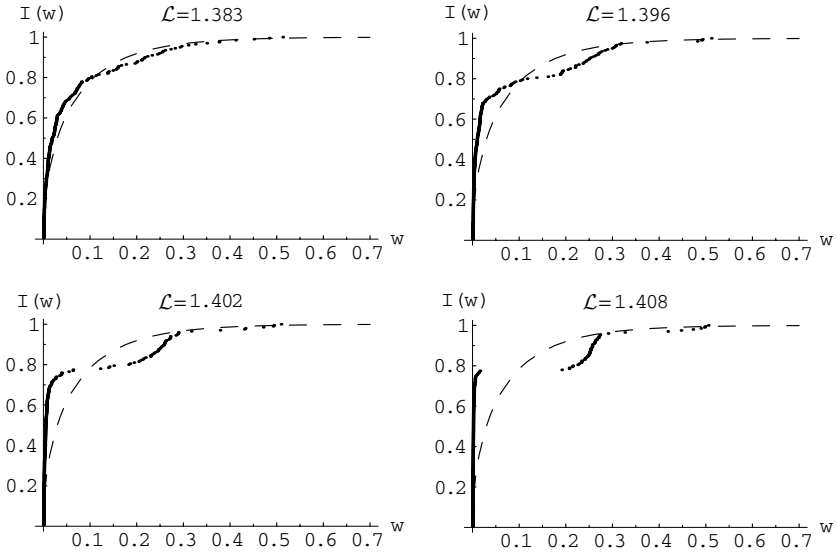

Figure 5. Integrated width density of 200 resonances for $\mathcal{L}$ between 1.383 and 1.408. The dashed curve is the integrated Porter–Thomas distribution.

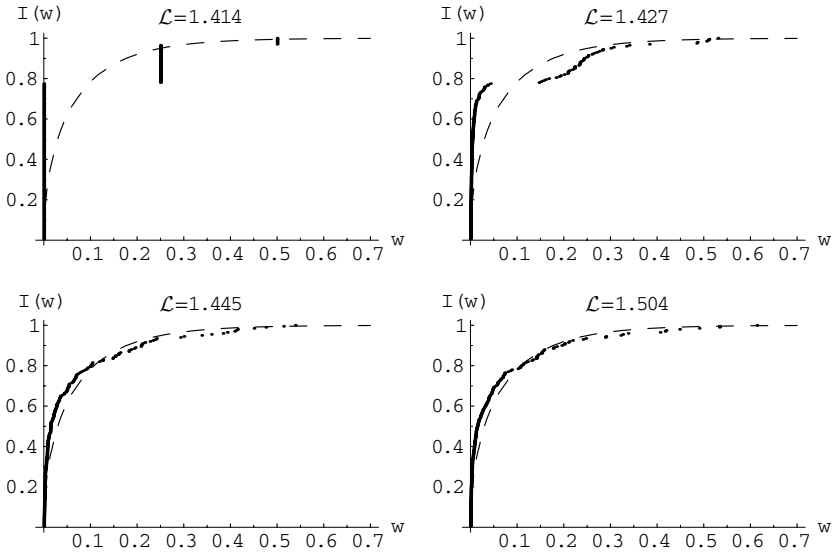

Figure 6. Integrated width density of 200 resonances for $\mathcal{L}$ between 1.414 and 1.504. The dashed curve is the integrated Porter–Thomas distribution. The case $\mathcal{L} = 1.414$ corresponds to the Hecke group with $\theta = \pi/4$.

demonstrate the return to the GOE behaviour in between. The case of $\mathcal{L} = 1.618, \theta = \pi/5$ shows reasonably good agreement with the GOE statistics. As with the widths, the billiard with $\mathcal{L} = 1.252$ appears to agree best with the GOE. In all the graphs, we additionally plot the integrated Poissonian (dashed curve) distribution

$$I(s) = 1 - \mathrm{e}^{-s}, \tag{53}$$

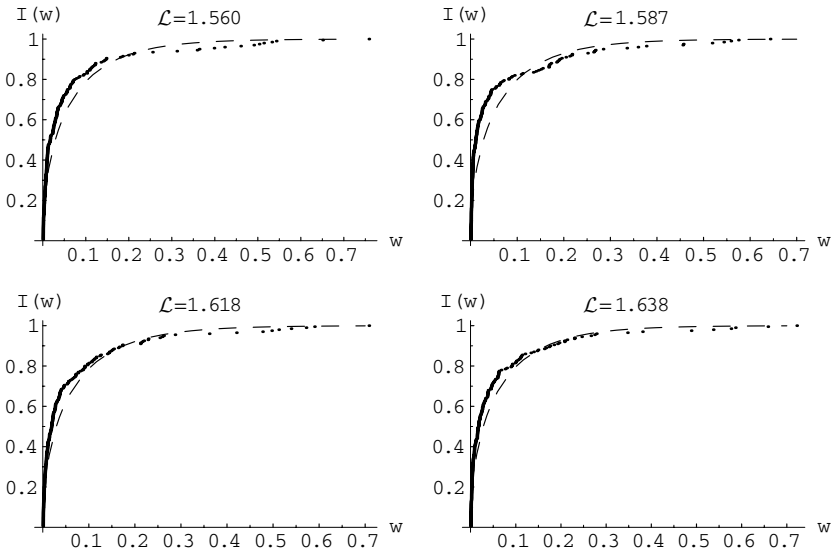

Figure 7. Integrated width density of 200 resonances for $\mathcal{L}$ between 1.560 and 1.638. The dashed curve is the integrated Porter–Thomas distribution. The case $\mathcal{L} = 1.618$ corresponds to the Hecke group with $\theta = \pi/5$. This is not an arithmetic group, but it tiles the plane.

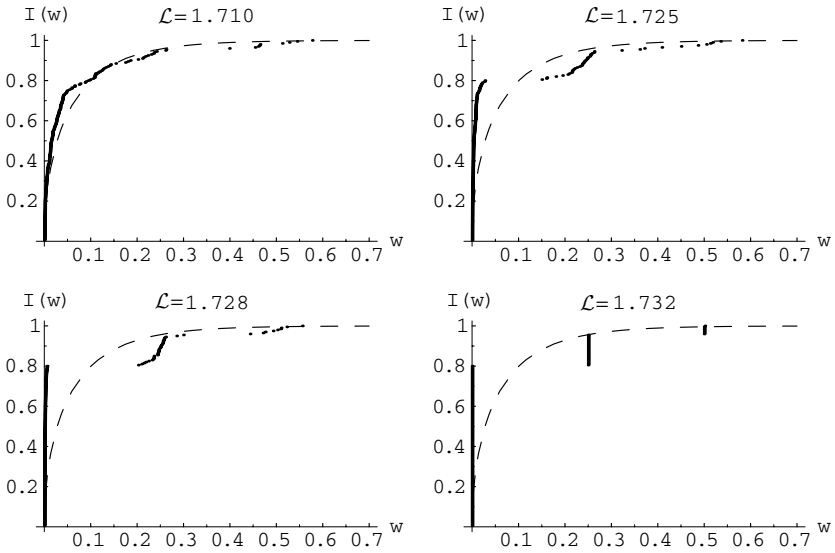

Figure 8. Integrated width density of 200 resonances for $\mathcal{L}$ between 1.710 and 1.732. The dashed curve is the integrated Porter–Thomas distribution. The case $\mathcal{L} = 1.732$ corresponds to the Hecke group with $\theta = \pi/6$.

which is predicted for generic integrable systems [35, 36]. Also shown are the integrated Wigner surmise for both the GOE (Gaussian orthogonal ensemble) (finely dashed curve)

$$I(s) = 1 - \mathrm{e}^{-\pi s^2/4} \tag{54}$$

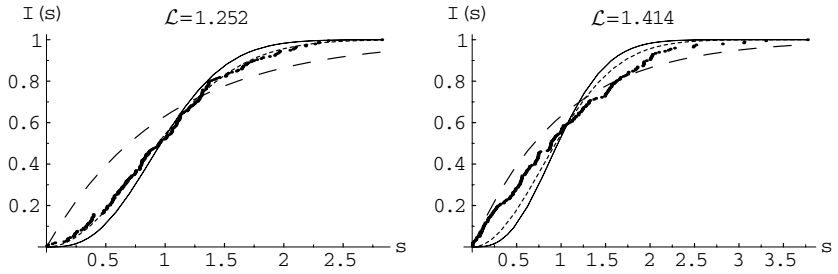

Figure 9. Integrated level-spacing distribution of 200 resonances for $\mathcal{L} = 1.252$ and $\mathcal{L} = \sqrt{2} \simeq 1.414$ ($\theta = \pi/4$). The dashed curve is the integrated Poisson distribution, the finely dashed curve is the GOE prediction and the solid curve is the GUE prediction.

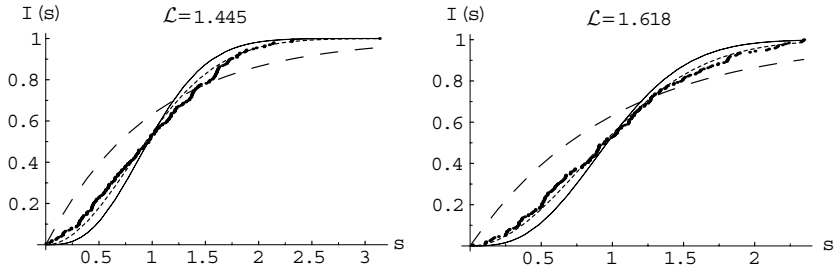

Figure 10. Integrated level-spacing distribution of 200 resonances for $\mathcal{L} = 1.445$ and $\mathcal{L} = 1.618$ ($\theta = \pi/5$). The dashed curve is the integrated Poisson distribution, the finely dashed curve is the GOE prediction and the solid curve is the GUE prediction.

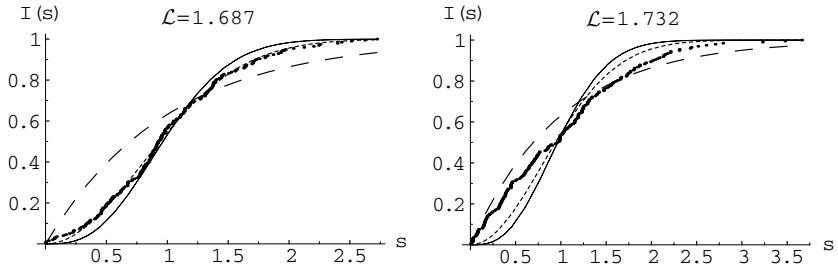

Figure 11. Integrated level-spacing distribution of 200 resonances for $\mathcal{L} = 1.687$ and $\mathcal{L} = \sqrt{3} \simeq 1.732$ ($\theta = \pi/6$). The dashed curve is the integrated Poisson distribution, the finely dashed curve is the GOE prediction and the solid curve is the GUE prediction.

and the GUE (Gaussian unitary ensemble) (solid curve)

$$I(s) = -\frac{4}{\pi} s\, \mathrm{e}^{-\frac{4}{\pi}s^2} + \mathrm{erf}(2s/\sqrt{\pi}), \tag{55}$$

which are very close to the distributions predicted for fully chaotic systems with time-reversal invariance and broken time-reversal invariance, respectively [8].

For the arithmetic cases, the distribution is essentially a weighted mixture of the Poisson and GUE distributions as shown in [14].

The integrated level density of the Brody distribution is [37]

$$I(s, \nu) = \int_0^s p(x, \nu)\, \mathrm{d}x = 1 - \exp(-a(\nu)s^{\nu+1}). \tag{56}$$

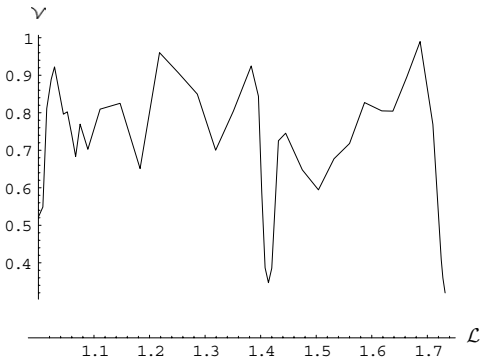

Figure 12. Variation of the Brody parameter ν with $\mathcal{L}$.

For $\nu = 0$ this gives (53) and for $\nu = 1$ (54) is obtained, and thus the Brody parameter ν serves as an empirical measure of how close a distribution is to either of those particular cases.

A least-squares fitting of the Brody parameter to our data was made and its variation followed, for the entire $\mathcal{L}$ range, in figure 12. The three transitions to arithmetic chaos are dramatically displayed as the sharp drops at $\mathcal{L} \in \{1, \sqrt{2}, \sqrt{3}\}$. These are mainly due to the large set of cusp forms with zero width and Poissonian statistics at these values. There appear to be lesser drops away from these special cases, but the current amount of data available does not make it possible to say much about them.

For bound systems, i.e. the odd spectrum, Bogomolny *et al* have shown that the non-generic behaviour displayed by arithmetic systems can be interpreted in terms of the Selberg trace formula, as being due to an exponential degeneracy in the number of periodic orbits with the same period [5]. Although such degeneracies persist for the Hecke group with $n = 5$, they are not large enough to affect the statistics, which are predicted to have the generic RMT behaviour. Our results indicate that the same holds true for open systems, i.e. the even spectra.

6. Conclusions

We have studied the behaviour of resonances for a class of billiard systems on the Poincaré half-plane. In particular, we have followed how the distributions of the positions and widths of the resonances move as the shape of Artin's billiard is perturbed by varying its width. Of particular interest were transitions in the distributions of the widths near values of the perturbation parameters which correspond to the underlying billiard being a fundamental domain for some arithmetic group. Analytic solutions for the resonances in these particular arithmetic systems were derived in section 3. While for most values of the perturbation parameters, the resonant energies distribute randomly according to the predictions of RMT, in these special cases three classes of resonance were observed: those which have zero imaginary part and become bound cusp forms; those with imaginary part equal to $-\frac{1}{4}$ positioned at half the magnitude of the Riemann zeros; and the class with imaginary part equal to $-\frac{1}{2}$ positioned at regular intervals of $\frac{2\pi}{\ln(\mathcal{L})}$.

For a general deformation, a specific numerical technique based on basis expansion collocation methods was developed to calculate the resonance positions and excellent agreement was obtained with the theory and the results of other groups, where they exist (see table 1). In the vast majority of parameter space, there are no other results in the literature for the resonance eigenvalues. Away from the arithmetic systems, largely generic behaviour

consistent with the predictions of RMT was observed. We also followed the variation of the Brody parameter characterizing the variation of the nearest-neighbour distribution of the resonance positions, and the scaling of this parameter under transitions to arithmetic chaos would also be of interest for further study. Preliminary results agreed well with those obtained elsewhere [38] for bound systems.

It has been seen that a spectral reorganization occurs in the arithmetic cases, where the S-matrix can be calculated analytically but not the cusp forms. This leads to non-generic statistics for the resonance levels and their widths. At first sight, the classical mechanics in arithmetic billiards seem no different from the generic case in that both have fully chaotic phase spaces. However, Bogomolny *et al* have shown [5] that in arithmetic cases there is an exponential degeneracy in the number of periodic orbits with the same period. This affects the Selberg trace formula [11] and hence the distribution of energy levels, leading to, in particular, Poissonian statistics for the cusp forms (they only studied bound systems). In addition, although there is a remaining exponential degeneracy for non-arithmetic cases with a smaller exponent, e.g. for the Hecke group with $n = 5$ above, they showed that the statistics in those cases appeared to be generic. For the open non-arithmetic systems studied here, and in particular for the Hecke triangular billiard $n = 5$, we find that both the level spacing statistics and the distribution of the widths are consistent with RMT for chaotic systems.

Acknowledgment

PJH was supported by an EPSRC postgraduate studentship.

Appendix. Calculation of Fourier coefficients with $m \neq 0$ in the case $\mathcal{L} = \sqrt{2}$

Starting from an expression for the mth Fourier coefficient of the wavefunction obtained by the method of images (16), which has a period $\mathcal{L}$, and using the substitution $s = 1/2 - \imath k$,

$$a_m(y) = \frac{1}{\sqrt{2}} \int_0^{\sqrt{2}} \sum_{\sigma \in \Gamma_0 \backslash \Gamma(2,4)} \frac{y^s}{|cz+d|^{2s}} \exp(-2\pi \imath m x/\sqrt{2})\, \mathrm{d}x. \tag{A.1}$$

The identity term in the sum gives a contribution $\delta_{0m}(y^{1-s})$ and using the right coset decomposition again, we get

$$a_m(y) = \frac{1}{\sqrt{2}} \int_{-\infty}^{\infty} \sum_{\sigma \in \Gamma_0 \backslash \Gamma(2,4)/\,\Gamma_0 - \mathbb{I}} \frac{y^s}{|cz+d|^{2s}} \exp(-2\pi \imath m x/\sqrt{2})\, \mathrm{d}x, \qquad m \neq 0. \tag{A.2}$$

Factoring out the arithmetic term from the integral as before, and performing the same substitutions on the latter, this becomes

$$a_m(y) = \sum_{c>0} \frac{1}{|c|^{2s}} \sum_{0 \leqslant d < \sqrt{2}c \,|\, ad-bc=1} \exp(-2\pi \imath m y d/\sqrt{2}c) \frac{y^{1-s}}{\sqrt{2}} \times \int_{-\infty}^{\infty} \frac{\exp(-2\pi \imath m y t/\sqrt{2})}{(1+t^2)^{2s}}\, \mathrm{d}t, \qquad m \neq 0. \tag{A.3}$$

The integral gives (see, e.g. [16]) a Bessel function,

$$\frac{y^{1-s}}{\sqrt{2}} \int_{-\infty}^{\infty} \frac{\exp(-2\pi \imath m y t/\sqrt{2})}{(1+t^2)^{2s}} \mathrm{d}t = \frac{1}{\sqrt{2}} 2\pi^s \left| \frac{m}{\sqrt{2}} \right|^{s-\frac{1}{2}} \Gamma(s)^{-1} \sqrt{y} \mathrm{K}_{s-\frac{1}{2}}(2\pi m y/\sqrt{2}), \qquad m \neq 0, \tag{A.4}$$

and we are just left with the arithmetic factor

$$\sum_{c>0} \frac{1}{|c|^{2s}} \sum_{0\leqslant d<\sqrt{2}c|ad-bc=1} \exp(-2\pi\imath md/\sqrt{2}c). \tag{A.5}$$

This factors, as in the case of a_0, into two sums over the two classes of matrix representation of the group $\Gamma(2,4)$, (14) and (15).

$$\begin{aligned}\sum_{c>0} \frac{1}{|c|^{2s}} &\sum_{0\leqslant d<\sqrt{2}c|ad-bc=1} \exp(-2\pi\imath md/\sqrt{2}c) \\ &= \sum_{c>0\in\mathbb{Z}} \frac{1}{|\sqrt{2}c|^{2s}} \sum_{0\leqslant d<2c\in\mathbb{Z}|(2c,d)=1} \exp(-2\pi\imath md/2c) \\ &\quad + \sum_{c\geqslant 0\in\mathbb{Z}} \frac{1}{|2c+1|^{2s}} \sum_{0\leqslant d<2c+1\in\mathbb{Z}|(2c+1,d)=1} \exp(-2\pi\imath md/(2c+1)),\end{aligned} \tag{A.6}$$

which gives

$$\sum_{\text{even } c>0} \frac{2^s}{|c|^{2s}} \sum_{0\leqslant d<c\in\mathbb{Z}|(c,d)=1} \exp(-2\pi\imath md/c) + \sum_{\text{odd } c} \frac{1}{|c|^{2s}} \sum_{0\leqslant d<c\in\mathbb{Z}|(c,d)=1} \exp(-2\pi\imath md/c). \tag{A.7}$$

Then using the identity

$$\sum_{0\leqslant d<c\in\mathbb{Z}} \exp(-2\pi\imath d/c) = 0, \tag{A.8}$$

we see that

$$\sum_{0\leqslant d<c\in\mathbb{Z}|(c,d)=1} \exp(-2\pi\imath md/c) = \sum_{u|m,u|c} u\mu(c/u), \tag{A.9}$$

where u are the mutual divisors of m and c, and $\mu(v)$ is the Möbius function,

$$\mu(v) = \begin{cases} 0, & \text{if } v \text{ has one or more repeated prime factors} \\ 1, & \text{if } v = 1 \\ (-1)^k, & \text{if } v \text{ is a product of } k \text{ distinct primes.} \end{cases} \tag{A.10}$$

This means we only sum over c of the form $c = uj$, $j \in \mathbb{Z}$ in (A.7), and the result is

$$\begin{aligned}\sum_{\text{even } ju>0} \frac{2^s}{|ju|^{2s}} \sum_{u|m} u\mu(j) &+ \sum_{\text{odd } ju} \frac{1}{|ju|^{2s}} \sum_{u|m} u\mu(j) \\ &= \sum_{\text{even } u|m} \sum_{j=1}^{\infty} \frac{2^s}{|ju|^{2s}} u\mu(j) + \sum_{\text{odd } u|m} \sum_{\text{even } j} \frac{2^s}{|ju|^{2s}} u\mu(j) + \sum_{\text{odd } u|m} \sum_{\text{odd } j} \frac{1}{|ju|^{2s}} u\mu(j).\end{aligned} \tag{A.11}$$

Then using the identity for the Riemann zeta function

$$\sum_{j} \frac{\mu(j)}{|j|^{2s}} = \zeta(2s)^{-1}, \tag{A.12}$$

and removing the respective odd or even terms as required from the sum, via the product representation

$$\zeta(2s)^{-1} = \prod_{p} \left(1 - \frac{1}{p^{2s}}\right), \tag{A.13}$$

where p here indicate the prime numbers, we arrive at our final result in the form of

$$a_m(y) = \frac{1}{\pi^{\imath k}\Gamma\left(\frac{1}{2}-\imath k\right)\zeta(1-2\imath k)(\sqrt{2}+2^{\imath k})} 2\sqrt{\pi}\left|\frac{m}{\sqrt{2}}\right|^{-\imath k}\sqrt{y}K_{-\imath k}(\sqrt{2}m\pi y) \times\left[2^{-\imath k}(\sqrt{2}+2^{\imath k})\sum_{\text{even } u|m} u^{2\imath k}+\sum_{\text{odd } u|m} u^{2\imath k}\right], \tag{A.14}$$

where we respecialized to $s = 1/2 - \imath k$.

A similar calculation can be performed for $a_m(y)$ for the $\mathcal{L} = \sqrt{3}$ case.

References

[1] Artin E 1924 *Abh. Math. Sem. d. Hamburgischen Universität* **3** 170–5
[2] Aurich R, Sieber M and Steiner F 1988 *Phys. Rev. Lett.* **61** 483–7
[3] Bohigas O, Giannoni M J and Schmit C 1986 *Quantum Chaos and Statistical Nuclear Physics (Lecture Notes in Physics* vol 263*)* (Berlin: Springer) pp 18–40
[4] Bogomolny E B, Georgeot B, Giannoni M J and Schmit C 1997 *Phys. Rep.* **291** 219–324
[5] Bogomolny E B, Georgeot B, Giannoni M J and Schmit C 1992 *Phys. Rev. Lett.* **69** 1477–80
[6] Bolte J, Steil G and Steiner F 1992 *Phys. Rev. Lett.* **69** 2188–91
[7] Gutzwiller M 1990 *Chaos in Classical and Quantum Mechanics* (Berlin: Springer)
[8] Stöckmann H J 1999 *Quantum Chaos: An Introduction* (Cambridge: Cambridge University Press)
[9] Friedrich H 1998 *Theoretical Atomic Physics* (Berlin: Springer)
[10] Phillips R S and Sarnak P 1985 *Commun. Pure Appl. Math.* **38** 853–66
[11] Balázs B V and Voros A 1986 *Phys. Rep.* **143** 109–240
[12] Hejhal D A 1992 *Mem. Am. Math. Soc.* **97** (469) 1–165
[13] Bogomolny E 2006 *Frontiers in Number Theory, Physics and Geometry, Proc. Les Houches Winter School 2003* (Berlin: Springer)
[14] Howard P J, Mota-Furtado F, O'Mahony P F and Uski V 2005 *J. Phys. A: Math. Gen.* **38** 10829–41
[15] Hejhal D 1983 *The Selberg Trace Formula for PSL(2, R)* vol 2 *(Springer Lecture Notes* vol 1001*)*
[16] Kubota T 1973 *Elementary Theory of Eisenstein Series* (New York: Wiley)
[17] Gutzwiller M C 1983 *Physica* D **7** 341–55
[18] Howard P J 2006 Resonance behaviour for classes of billiards on the Poincaré half-plane *PhD thesis* Royal Holloway, University of London
[19] Gaspard P and Rice S 1989 *J. Chem. Phys.* **90** 2242–54
[20] Titchmarsh E C 1951 *The Theory of the Riemann Zeta-Function* (Oxford: Oxford University Press)
[21] Arfken G 1985 *Mathematical Methods for Physicists* (New York: Academic) pp 560–62
[22] Schmit C 1980 *Chaos et Physique Quantique—Chaos and Quantum Physics, Les Houches, ecole d'éte de physique theorique 1989, session LII* (Amsterdam: Elsevier)
[23] Graham R, Hübner R, Szépfalusy P and Vattay G 1991 *Phys. Rev.* A **44** 7002–15
[24] Alt H, Dembowski C, Gräf H D, Hofferbert R, Rehfeld H, Richter A and Schmit C 1999 *Phys. Rev.* E **60** 2851–7
[25] Backer A 2003 *The Mathematical Aspects of Quantum Maps* ed M D Esposti and S Graffi (Berlin: Springer)
[26] Anderson E *et al* 1999 *LAPACK Users' Guide* 3rd edn (Society for Industrial and Applied Mathematics)
[27] Abramowitz M and Stegun I A 1965 *Handbook of Mathematical Functions* (New York: Dover)
[28] Then H 2005 *Math. Comput.* **74** 363–81
[29] Steil G 1994 Eigenvalues of the Laplacian and of the Hecke operators for PSL(2, $\mathbb{Z}$) Tech. Rep. DESY
[30] Hejhal D A and Berg B 1982 Some new results concerning eigenvalues of the non-Euclidean Laplacian for PSL(2, $\mathbb{Z}$) Tech. Rep. University of Minnesota
[31] Odlyzko A M The first 100,000 zeros of the Riemann zeta function, accurate to within $3 * 10^{-9}$ http://www.dtc.umn.edu/~odlyzko/zeta_tables/zeros1
[32] Wardlaw D M and Jaworski W 1989 *J. Phys. A: Math. Gen.* **22** 3561–75
[33] Bogomolny E B and Schmit C 2004 *J. Phys. A: Math. Gen.* **37** 4501–26
[34] Sieber M, Smilansky U, Creagh S and Littlejohn R G 1993 *J. Phys. A: Math. Gen.* **26** 6217–30
[35] Berry M V and Tabor M 1977 *Proc. R. Soc. Lond.* **356** 375–94
[36] Robnik M and Veble G 1998 *J. Phys. A: Math. Gen.* **31** 4669–704
[37] Brody T A 1973 *Lett. Nuovo Cimento* **7** 482
[38] Csordás A, Graham R, Szépfalusy P and Vattay G 1994 *Phys. Rev.* E **49** 325–33